J. Fluid Mech. (2000), *vol.* 421, *pp.* 115–145. Printed in the United Kingdom

A theory for turbulent pipe and channel flows

By MARTIN WOSNIK[1], LUCIANO CASTILLO[2] AND WILLIAM K. GEORGE[3]

[1]State University of New York at Buffalo, Buffalo, NY 14260, USA

[2]Rensselaer Polytechnic Institute, Troy, NY 12180, USA

[3]Department of Thermo and Fluid Dynamics, Chalmers University of Technology, 412 96 Göteborg, Sweden

(Received 28 January 1998 and in revised form 14 February 2000)

A theory for fully developed turbulent pipe and channel flows is proposed which extends the classical analysis to include the effects of finite Reynolds number. The proper scaling for these flows at finite Reynolds number is developed from dimensional and physical considerations using the Reynolds-averaged Navier–Stokes equations. In the limit of infinite Reynolds number, these reduce to the familiar law of the wall and velocity deficit law respectively.

The fact that both scaled profiles describe the entire flow for finite values of Reynolds number but reduce to inner and outer profiles is used to determine their functional forms in the 'overlap' region which both retain in the limit. This overlap region corresponds to the constant, Reynolds shear stress region ($30 < y^+ < 0.1R^+$ approximately, where $R^+ = u_* R/\nu$). The profiles in this overlap region are logarithmic, but in the variable $y + a$ where a is an offset. Unlike the classical theory, the additive parameters, B_i, B_o, and log coefficient, $1/\kappa$, depend on R^+. They are asymptotically constant, however, and are linked by a constraint equation. The corresponding friction law is also logarithmic and entirely determined by the velocity profile parameters, or vice versa.

It is also argued that there exists a *mesolayer* near the bottom of the overlap region approximately bounded by $30 < y^+ < 300$ where there is not the necessary scale separation between the energy and dissipation ranges for inertially dominated turbulence. As a consequence, the Reynolds stress and mean flow retain a Reynolds number dependence, even though the terms explicitly containing the viscosity are negligible in the single-point Reynolds-averaged equations. A simple turbulence model shows that the offset parameter a accounts for the mesolayer, and because of it a logarithmic behaviour in y applies only beyond $y^+ > 300$, well outside where it has commonly been sought.

The experimental data from the superpipe experiment and DNS of channel flow are carefully examined and shown to be in excellent agreement with the new theory over the entire range $1.8 \times 10^2 < R^+ < 5.3 \times 10^5$. The Reynolds number dependence of all the parameters and the friction law can be determined from the single empirical function, $H = A/(\ln R^+)^\alpha$ for $\alpha > 0$, just as for boundary layers. The Reynolds number dependence of the parameters diminishes very slowly with increasing Reynolds number, and the asymptotic behaviour is reached only when $R^+ \gg 10^5$.

1. Introduction

Pipe and channel flows have recently become the subject of intense scrutiny, thanks in part to new experimental data which has become available from the superpipe experiment at Princeton (Zagarola 1996; Zagarola & Smits 1998*a*). In spite of the facts that the scaling laws for pipe and channel flows were established more than 80 years ago (Stanton & Pannell 1914; Prandtl 1932) and that the now classical theory of Millikan was offered in 1938 for the friction law and velocity profiles, the subject has remained of considerable interest. Examples from the last 30 years alone include the analyses of Tennekes (1968), Bush & Fendell (1974), Long & Chen (1981), and Panton (1990). All of these were essentially refinements of the original Millikan theory in which the essential functional form of the friction and velocity laws was logarithmic, and only the infinite Reynolds number state was considered. The difficulties presented by the experimental data have recently been extensively reviewed by Gad-el-Hak & Bandyopadhyay (1994).

Barenblatt and coworkers (Barenblatt 1993, 1996; Barenblatt & Prostokishin 1993; Barenblatt, Chorin & Prostokishin 1997) have suggested that the velocity profiles of pipe, channel and boundary layer flows are power laws. By contrast, George and coworkers (George 1988, 1990, 1995; George & Castillo 1993, 1997; George, Knecht & Castillo 1992; George, Castillo & Knecht 1996; George, Castillo & Wosnik 1997) have argued that the overlap velocity profiles and friction law for boundary layers are power laws, but that the corresponding relations for pipes and channels are logarithmic.

Specifically, for boundary layers George & Castillo (1997 hereafter referred to as GC), used the Reynolds-averaged Navier–Stokes equations and an asymptotic invariance principle (AIP) to deduce that the proper velocity scale for the outer part was U_∞, the free-stream velocity. In the inner region, however, the proper velocity scale was u_*, the friction velocity, just as in the classical law of the wall. Since the ratio u_*/U_∞ varied with Reynolds number, so did the velocity profiles in the *Reynolds number dependent* overlap region. These were derived using near asymptotics as

$$\frac{U}{u_*} = C_i(y^+ + a^+)^\gamma \tag{1.1}$$

and

$$\frac{U}{U_\infty} = C_o(\overline{y} + \overline{a})^\gamma, \tag{1.2}$$

where $y^+ = y/\eta$, $\eta = \nu/u_*$, $\overline{y} = y/\delta$ where δ is the boundary layer thickness (chosen as $\delta_{0.99}$ for convenience). This overlap region was shown to correspond to the region of constant Reynolds stress of the flow, approximately $30 < y^+ < 0.1\delta^+$. The parameter a represents an origin shift, and was shown to be related to the existence of a mesolayer in the region approximately given by $30 < y^+ < 300$ in which the dissipative scales are not fully separated from the energy and Reynolds stress producing ones.

The parameters C_i, C_o, and γ were functions of δ^+, were asymptotically constant, and satisfied the constraint equation,

$$\ln \delta^+ \frac{\mathrm{d}\gamma}{\mathrm{d}\ln\delta^+} = \frac{\mathrm{d}\ln C_o/C_i}{\mathrm{d}\ln\delta^+} \tag{1.3}$$

where $\delta^+ = u_*\delta/\nu$. The friction law was given by

$$\frac{u_*}{U_\infty} = \frac{C_o}{C_i}(\delta^+)^{-\gamma}. \tag{1.4}$$

The constraint equation was transformed by defining a single new function $h = h(\ln \delta^+)$

$$\ln C_o/C_i = (\gamma - \gamma_\infty) \ln \delta^+ + h \tag{1.5}$$

and

$$\gamma - \gamma_\infty = -\frac{\mathrm{d}h}{\mathrm{d} \ln \delta^+}. \tag{1.6}$$

The function $h - h_\infty$ was determined empirically to be given by

$$h(\delta^+) - h_\infty = \frac{A}{(\ln \delta^+)^\alpha}, \tag{1.7}$$

where $h_\infty = \ln(C_{o\infty}/C_{i\infty})$ and $\alpha > 1$ is a necessary condition. (Note that this can be shown to be the leading term in an expansion of the exact solution.)

It followed immediately that

$$\gamma - \gamma_\infty = \frac{\alpha A}{(\ln \delta^+)^{1+\alpha}}, \tag{1.8}$$

$$\frac{C_o}{C_i} = \frac{C_{o\infty}}{C_{i\infty}} \exp[(1+\alpha)A/(\ln \delta^+)^\alpha] \tag{1.9}$$

and

$$\frac{u_*}{U_\infty} = \frac{C_{o\infty}}{C_{i\infty}} (\delta^+)^{-\gamma_\infty} \exp[A/(\ln \delta^+)^\alpha]. \tag{1.10}$$

The values for the constants were determined from the data to be $\gamma_\infty = 0.0362$, $C_{o\infty}/C_{i\infty} = \exp(h_\infty) = 0.0163$, $C_o \approx C_{o\infty} = 0.897$ (so $C_{i\infty} = 55$), $A = 2.9$, and $\alpha = 0.46$. Also it was established from the available data that a^+ was nearly constant and approximately equal to -16.

The purpose of this paper is to apply the same methodology to pipe and channel flows, and to compare the resulting theory with the new experimental data. The important difference from previous efforts mentioned above will be seen to be that the effects of finite Reynolds number are explicitly included and the mesolayer is accounted for.

2. Scaling laws for turbulent pipe and channel flow

The streamwise momentum equation for a fully developed two-dimensional channel flow at high Reynolds number reduces to

$$0 = -\frac{1}{\rho}\frac{\mathrm{d}P}{\mathrm{d}x} + \frac{\partial}{\partial y}\left[\langle -uv \rangle + \nu \frac{\partial U}{\partial y}\right]. \tag{2.1}$$

Like the boundary layer, the viscous term is negligible everywhere except very near the wall, so that the core (or outer) flow in the limit of infinite Reynolds number is exactly governed by

$$0 = -\frac{1}{\rho}\frac{\mathrm{d}P}{\mathrm{d}x} + \frac{\partial}{\partial y}\langle -uv \rangle. \tag{2.2}$$

In the limit of infinite Reynolds number, the inner layer is exactly governed by

$$0 = \frac{\partial}{\partial y}\left[\langle -uv \rangle + \nu \frac{\partial U}{\partial y}\right]. \tag{2.3}$$

This can be integrated from the wall to obtain the total stress

$$u_*^2 = \langle -uv \rangle + \nu \frac{\partial U}{\partial y}, \tag{2.4}$$

where u_* is the friction velocity defined as $u_*^2 \equiv \tau_w/\rho$. As the distance from the wall is increased, the viscous stress vanishes and $\langle -uv \rangle \to u_*^2$, but only in the infinite Reynolds number limit. At finite Reynolds numbers the pressure gradient causes the total stress to drop linearly until it reaches zero at the centre of the channel (or pipe). Hence the Reynolds stress never really reaches the value of u_*^2, but instead reaches a maximum value away from the wall before dropping slowly as distance from the wall is increased.

It is obvious that the inner profiles must scale with u_* and ν since these are the only parameters in the inner equations and boundary conditions. Hence, there must be a law of the wall (at least for a limited region very close to the wall). This should not be taken to imply, however, that u_*^2 is an independent parameter; it is not. It is uniquely determined by the pressure drop imposed on the pipe, the pipe diameter and the kinematic viscosity.

Because there is no imposed condition on the velocity, except for the no-slip condition at the wall, an outer scaling velocity must be sought from the parameters in the outer equation itself. Since there are only two, $-(1/\rho)\mathrm{d}P/\mathrm{d}x$, the externally imposed pressure gradient, and R, the channel half-width, only a single velocity can be formed, namely

$$U_o = \left(-\frac{R}{\rho} \frac{\mathrm{d}P}{\mathrm{d}x} \right)^{1/2}. \tag{2.5}$$

Unlike the developing boundary layer, the fully developed pipe or channel flow is homogeneous in the streamwise direction, so the straightforward similarity analysis of GC using the x-dependence to establish the scaling parameters is not possible. However, because of this streamwise homogeneity, there is an exact balance between the wall shear stress acting on the walls, and the net pressure force acting across the flow. For fully developed channel flow, this equilibrium requires that

$$u_*^2 = -\frac{R}{\rho} \frac{\mathrm{d}P}{\mathrm{d}x}. \tag{2.6}$$

which is just the square of equation (2.5) above; thus, $U_o = u_*$. Therefore, the outer scale velocity is also u_*, and the outer and inner velocity scales are the same. The factor of 2 which appears in the corresponding pipe flow force balance can be ignored in choosing the scale velocity, so the same argument and result apply to it as well.

Thus channel and pipe flows differ from boundary layer flows where asymptotic Reynolds number independence and streamwise *inhomogeneity* demand that the inner and outer scales for the mean velocity be different (GC). This consequence of the streamwise homogeneity for the governing equations themselves is fundamental to understanding the unique nature of pipe and channel flows. Homogeneity causes the inner and outer velocity scale to be the same, and this in turn is the reason why these flows show a logarithmic dependence for the velocity in the overlap region and for the friction law. This can be contrasted with boundary layers, where the inner and outer velocity scales are different because of their inhomogeneity in x, and hence are characterized by power laws.

The analysis presented below will be based on using u_* as the outer velocity scale; however, it should be noted before leaving this section that there are at least two

other possibilities which might be considered for an outer velocity scale. Both are formed from the mass-averaged velocity defined for the pipe by

$$U_m \equiv \frac{1}{\pi R^2}\int_0^R U r \mathrm{d}r. \tag{2.7}$$

The first possibility is to use U_m directly, the second is to use its difference from the centreline velocity, $U_c - U_m$. The former has an advantage in that it is often easier to specify the mass flow in experiments and simulations than the pressure drop (or shear stress), but it has the disadvantage that it does not lend itself easily to the overlap analysis described below. The latter has been utilized with great success by Zagarola & Smits (1998*b*) in removing the Reynolds number dependence of the velocity profiles in both boundary layers and pipe flows. For the purpose of this paper it is sufficient to note that in the limit as $R^+ = u_* R/\nu \to \infty$, $U_c - U_m \to \text{const} \times u_*$. Hence the fundamental limiting and overlap arguments of the succeeding sections will be the same for both u_* and $U_c - U_m$; only the Reynolds number dependence of the coefficients will differ.

3. Finite versus infinite Reynolds number

From the dimensional/physical analysis above, it follows that appropriate inner- and outer-scaled versions of the velocity profile can be defined as two families of curves with parameter R^+, i.e.

$$\frac{U}{u_*} = f_i(y^+, R^+) \tag{3.1}$$

and

$$\frac{U - U_c}{u_*} = f_o(\overline{y}, R^+), \tag{3.2}$$

where the outer velocity has been referenced to the velocity at the centreline, U_c, to avoid the necessity of accounting for viscous effects over the inner layer when the limits are taken later. The outer length scale is some measure of the diameter of the pipe (say the pipe radius) or the width of the channel (say half-width). Both of these will be denoted as R in the remainder of the paper.

Since the length scales for inner and outer profiles are different, no single scaling law should be able to collapse data for the entire flow. The ratio of length scales is a Reynolds number, $R^+ = Ru_*/\nu$, therefore the region between the two similarity regimes cannot be Reynolds number independent, except possibly in the limit of infinite Reynolds number. Moreover, since the neglected terms in both inner and outer equations depend on the ratio of length scales (see Tennekes & Lumley 1972), then neither set of scaling parameters will be able to perfectly collapse the data in either region at finite values of R^+.

The actual mean velocity profile at finite Reynolds number is the average of the instantaneous solutions to the Navier–Stokes equations and boundary conditions. This profile, whether determined from a real flow by measurement, a direct numerical simulation, or not at all, exists, at least in principle, and is valid everywhere *regardless of how it is scaled*. Therefore it is important to note that both families of curves described by equations (3.1) and (3.2), $f_i(y^+, R^+)$ and $f_o(\overline{y}, R^+)$, represent the entire velocity profile, at least as long as the dependence on R^+ is retained (as long as R^+ is finite). In other words, they represent the same solutions, and have simply been scaled differently.

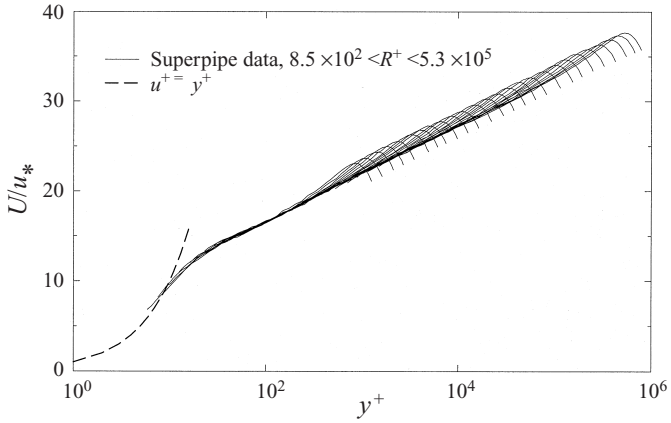

FIGURE 1. Velocity profiles in inner variables.

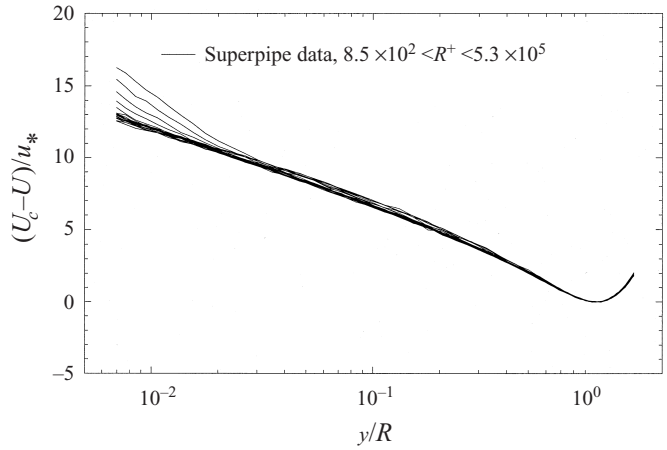

FIGURE 2. Velocity profiles in outer variables.

Properly scaled profiles must, by the asymptotic invariance principle (AIP, George 1995), become asymptotically independent of R^+ in the limit of infinite Reynolds number, i.e.

$$\lim f_i(y^+, R^+) \to f_{i\infty}(y^+),$$
$$\lim f_o(\overline{y}, R^+) \to f_{o\infty}(\overline{y})$$

as $R^+ \to \infty$. Otherwise an inner and outer scaling makes no sense. In fact, these limiting profiles should be solutions to the inner and outer equations respectively (i.e. equations (2.3) and (2.2)), which are themselves valid only in the infinite Reynolds number limit.

Figures 1 and 2 show the mean velocity profile data from the Princeton superpipe experiment (Zagarola 1996; Zagarola & Smits 1998*a*) in both inner and outer variables. Note the excellent collapse very close to the wall for $y^+ < 100$ in inner variables, and over the core region for $\overline{y} > 0.3$. Note also that the region of approximate collapse in inner variables (figure 1) increases from the wall with increasing Reynolds number, as does the inward extent of the outer variable collapse (figure 2). In fact, the parameter R^+ uniquely labels the fanning out of the inner-scaled profiles in the outer region and the outer-scaled profiles near the wall in figures 1 and 2.

Finally note that the inner scaling does not collapse the data at all where the outer scaling collapses it best, and vice versa. Both the region of approximate collapse and the region of no collapse are manifestations of the dependence of the scaled profiles on R^+ as argued above.

Unlike boundary layer experiments, the wall shear stress for the fully developed pipe flow can be determined from the pressure drop in the pipe alone, entirely independent of the velocity profile measurements. The direct determination of the shear stress from the pressure drop without choosing it to collapse a 'log layer' which can only be assumed to collapse (the so-called 'Clauser method') is especially important since, as noted above, there is evidence of a lack of complete collapse of the data in figure 1 outside $y^+ = 100$, especially for the lowest Reynolds numbers. The lack of collapse is even more apparent for the outer scaling in figure 2 inside $\overline{y} \approx 0.3$ which includes all of the overlap region discussed below.

4. The overlap layer: an application of near asymptotics

As discussed in the preceding section, f_i and f_o are quite unlike their limiting forms, $f_{i\infty}$ and $f_{o\infty}$, which are only infinite Reynolds number solutions for the inner and outer equations respectively. If f_i and f_o are considered instead of $f_{i\infty}$ and $f_{o\infty}$ (as is usually done), the problem of determining whether an overlap region exists is quite different from the usual asymptotic matching where infinite Reynolds number inner and outer solutions are extended and matched in an overlap region if one exists. The objective here is not to see if f_i and f_o overlap and match them if they do. Rather, it is to determine *whether* the fact that *these scaled finite Reynolds number solutions* (*to the whole flow*) *degenerate at infinite Reynolds number in different ways* can be used to determine their functional forms in the common region they retain in the limit. The methodology, termed *near asymptotics*, was first utilized by George (1995) (see also GC), and is necessary because the traditional approach cannot account for the possibility of the matching parameter tending to zero, as might be the case. It also makes the results easier to compare to experiments since most are carried out far from asymptotic conditions.

The fact that analytical forms for f_i and f_o are not available, and they are only known in principle turns out not to be a significant handicap. There are several pieces of information about the two profiles which can be utilized without further assumptions. They are:

First, since both inner and outer forms of the velocity profile must describe the flow everywhere as long as the ratio of length scales, $R^+ = R/\eta$, is finite, it follows from equations (3.1) and (3.2) that

$$\frac{1}{g(R^+)} + f_o(\overline{y}, R^+) = f_i(y^+, R^+), \tag{4.1}$$

where $g(R^+)$ is defined by

$$g(R^+) \equiv u_*/U_c. \tag{4.2}$$

Second, for finite values of R^+, the velocity derivatives from both inner and outer forms of the velocity must also be the same everywhere. This implies that

$$\overline{y}\frac{\partial f_o}{\partial \overline{y}} = y^+\frac{\partial f_i}{\partial y^+} \tag{4.3}$$

for all values of R^+ and y.

Third, as noted above, in the limit both f_o and f_i must become asymptotically independent of R^+, i.e. $f_o(\overline{y}, R^+) \to f_{o\infty}(\overline{y})$ and $f_i(y^+, R^+) \to f_{i\infty}(y^+)$ as $R^+ \to \infty$.

Now the problem is that in the limit as $R^+ \to \infty$, the outer form fails to account for the behaviour close to the wall while the inner form fails to describe the behaviour away from it. The question is: In this limit (as well as for all finite values approaching it) does there exist an 'overlap' region where equation (4.1) is still valid? (Note that boundary layer flows are quite different from pipe and channel flows since the overlap layer in the latter remains at fixed distance from the wall for all x because of the streamwise homogeneity, as long as the external parameters – like geometry and Reynolds number – are fixed, while in the former it moves away from the wall with increasing x.)

The question of whether there is a common region of validity can be investigated by examining how rapidly f_o and f_i are changing with R^+, or more conveniently with $\ln R^+$. The relative variation of f_i and f_o with Reynolds number can be related to their Taylor series expansion about a fixed value of R^+, i.e.

$$\frac{f_i(y^+; R^+ + \Delta R^+) - f_i(y^+; R^+)}{\Delta \ln R^+ f_i(y^+, R^+)} \approx \frac{1}{f_i(y^+, R^+)} \frac{\partial f_i(y^+; R^+)}{\partial \ln R^+}\bigg|_{y^+} \equiv S_i(R^+, y^+) \tag{4.4}$$

and

$$\frac{f_o(\overline{y}; R^+ + \Delta R^+) - f_o(\overline{y}; R^+)}{\Delta \ln R^+ f_o(\overline{y}, R^+)} \approx \frac{1}{f_o(\overline{y}, R^+)} \frac{\partial f_o(\overline{y}; R^+)}{\partial \ln R^+}\bigg|_{\overline{y}} \equiv S_o(R^+, \overline{y}). \tag{4.5}$$

Thus S_i and S_o are measures of the Reynolds number dependence of f_i and f_o, respectively. Both vanish identically in the limit as $\ln R^+ \to \infty$. If y^+_{max} denotes a location where outer flow effects begin to be strongly felt on the inner-scaled profile, then for $y^+ < y^+_{max}$, S_i should be much less than unity (or else the inner scaling is not very useful). Similarly, if $\overline{y}_{min}$ measures the location where viscous effects begin to be strongly felt (e.g. as the linear velocity region near the wall is approached), then S_o should be small for $\overline{y} > \overline{y}_{min}$. Obviously either S_i or S_o should increase as these limits are approached. Outside these limits, one or the other should increase dramatically.

The quantities S_i and S_o can, in fact, be used to provide a formal definition of an 'overlap' region where both scaling laws are valid. Since S_i will increase drastically for large values of y for given $\ln R^+$, and S_o will increase for small values of y, an 'overlap' region exists only if there is a region for which both S_i and S_o remain small simultaneously. In the following paragraphs, this condition will be used in conjunction with equation (4.1) to derive the functional form of the velocity in the overlap region *at finite Reynolds number*, hence the term 'near asymptotics'.

Because the overlap region moves toward the wall with increasing R^+, it is convenient and necessary to introduce an intermediate variable $\tilde{y}$ which can be fixed in the overlap region all the way to the limit, regardless of what is happening in physical space (see Cole & Kevorkian 1981). A definition of $\tilde{y}$ which accomplishes this is given by

$$\tilde{y} = y^+ R^{+-n} \tag{4.6}$$

or

$$y^+ = \tilde{y} R^{+n}. \tag{4.7}$$

Since $R^+ = y^+/\overline{y}$, it follows that

$$\overline{y} = \tilde{y} R^{+n-1}. \tag{4.8}$$

For all values of n satisfying $0 < n < 1$, $\tilde{y}$ can remain fixed in the limit as $R^+ \to \infty$

while $\overline{y} \to 0$ and $y^+ \to \infty$. Substituting these into equation (4.1) yields the matching condition on the velocity in terms of the intermediate variable:

$$\frac{1}{g(R^+)} + f_o(R^{+n-1}\tilde{y}, R^+) = f_i(R^{+n}\tilde{y}, R^+). \tag{4.9}$$

Now equation (4.9) can be differentiated with respect to R^+ for fixed $\tilde{y}$ to yield equations which explicitly include S_i and S_o. The result after some manipulation is

$$\overline{y}\frac{\partial f_o}{\partial \overline{y}}\bigg|_{R^+} = \frac{1}{\kappa} - \left[S_i(y^+, R^+)f_i(y^+, R^+) - S_o(\overline{y}, R^+)f_o(\overline{y}, R^+)\right], \tag{4.10}$$

where

$$\frac{1}{\kappa(R^+)} \equiv -\frac{R^+}{g^2}\frac{\mathrm{d}g}{\mathrm{d}R^+} = \frac{\mathrm{d}(1/g)}{\mathrm{d}\ln R^+}. \tag{4.11}$$

The first term on the right-hand side of equation (4.10) is at most a function of R^+ alone, while the second term contains all of the residual y-dependence.

Now it is clear that if both

$$|S_o|\, f_o \ll 1/\kappa \tag{4.12}$$

and

$$|S_i|\, f_i \ll 1/\kappa \tag{4.13}$$

then the first term on the right-hand side of equation (4.10) dominates. If $1/\kappa \to 0$, the inequalities are still satisfied as long as the left-hand side of equations (4.12) and (4.13) does so more rapidly than $1/\kappa$. Note that a much weaker condition can be applied which yields the same result, namely that both inner and outer scaled profiles have the same dependence on R^+, i.e. $S_i f_i = S_o f_o$ in the overlap range so only $1/\kappa$ remains. If these inequalities are satisfied over some range in y, then to leading order, equation (4.10) can be written as

$$\overline{y}\frac{\partial f_o}{\partial \overline{y}}\bigg|_{R^+} = \frac{1}{\kappa}. \tag{4.14}$$

The solution to equation (4.14) could be denoted as $f_o^{(1)}$ since it represents a first-order approximation to f_o. Because $1/\kappa$ depends on R^+ it is not simply the same as $f_{o\infty}$, but reduces to it in the limit. Thus, by regrouping all of the y-independent contributions into the leading term, the method applied here has yielded a more general result than the customary expansion about infinite Reynolds number. (It is also easy to see why the usual matching of infinite Reynolds number inner and outer solutions will not work if the limiting value of $1/\kappa$ is zero, which cannot yet be ruled out.)

From equations (4.3) and (4.14), it follows that

$$y^+\frac{\partial f_i}{\partial y^+}\bigg|_{R^+} = \frac{1}{\kappa}. \tag{4.15}$$

Equations (4.14) and (4.15) must be independent of the origin for y; hence they must be invariant to transformations of the forms $\overline{y} \to \overline{y} + \overline{a}$ and $y^+ \to y^+ + a^+$, respectively, where a is at most a function of the Reynolds number. Therefore the most general forms of equations (4.14) and (4.17) are

$$(\overline{y} + \overline{a})\frac{\partial f_o}{\partial(\overline{y} + \overline{a})}\bigg|_{R^+} = \frac{1}{\kappa} \tag{4.16}$$

and

$$(y^+ + a^+)\frac{\partial f_i}{\partial(y^+ + a^+)}\bigg|_{R^+} = \frac{1}{\kappa}. \tag{4.17}$$

The solutions to these overlap equations are given by

$$\frac{U - U_c}{u_*} = f_o(\overline{y}, R^+) = \frac{1}{\kappa(R^+)}\ln[\overline{y} + \overline{a}(R^+)] + B_o(R^+) \tag{4.18}$$

and

$$\frac{U}{u_*} = f_i(y^+, R^+) = \frac{1}{\kappa(R^+)}\ln[y^+ + a^+(R^+)] + B_i(R^+). \tag{4.19}$$

The superscript (1) has been dropped; however it is these first-order solutions that are being referred to unless otherwise stated. Thus the velocity profiles in the overlap region are logarithmic, but with parameters which are in general Reynolds number dependent.

Note that the particular form of the solution $\ln(y + a)$ has also been identified by Oberlack (1997) from a Lie group analysis of the equations governing homogeneous shear flows. It will be argued in § 8 that a^+ is closely related to the *mesolayer*, just as it is for the boundary layer (GC). The data will be found to be consistent with $a^+ \approx -8$. Interestingly, the need for the offset parameter a appears to have first been noticed by Squire (1948) (see also Duncan, Thom & Young 1970) using a simple eddy viscosity model. (Even his value of $a^+ = 5.9$ does not differ much from the one used here.) George *et al.* (1996) arrived at a similar form from a simple one-equation turbulence model for the mesolayer, as discussed in § 8 below.

A particularly interesting feature of these first-order solutions is that the inequalities given by equations (4.12) and (4.13) determine the limits of validity of both equations (4.16) and (4.17) since either S_o or S_i will be large outside the overlap region. Clearly, the extent of this region will increase as the Reynolds number (or R^+) increases.

The parameters $1/\kappa$, B_i and B_o must be asymptotically constant since they occur in solutions to equations which are themselves Reynolds number independent in the limit (AIP). Moreover, the limiting values, κ_∞, $B_{i\infty}$, and $B_{o\infty}$ cannot all be zero, or else the solutions themselves are trivial. In the limit of infinite Reynolds number the energy balance in the overlap region reduces to production equals dissipation, i.e. $\epsilon^+ = P^+$. In § 8 this will be shown to imply that

$$\epsilon^+ \to \frac{\mathrm{d}u^+}{\mathrm{d}y^+} = \frac{1}{\kappa(y^+ + a^+)}. \tag{4.20}$$

Since the local energy dissipation rate must be finite and non-zero (Frisch 1995), it follows that $1/\kappa_\infty$ must be finite and non-zero. It will be shown below that these conditions severely restrict the possible Reynolds number dependences for the parameters κ, B_i and B_o. (Note that the same physical constraint on the boundary layer results requires the power exponent, γ, to be asymptotically finite and non-zero.)

The relation between u_* and U_c follows immediately from equation (4.1), i.e.

$$\frac{U_c}{u_*} = \frac{1}{g(R^+)} = \frac{1}{\kappa(R^+)}\ln R^+ + [B_i(R^+) - B_o(R^+)]. \tag{4.21}$$

Thus the friction law is entirely determined by the velocity parameters for the overlap region. However, equation (4.11) must also be satisfied. Substituting

equation (4.21) into equation (4.11) implies that κ, B_i, and B_o are constrained by

$$\ln R^+ \frac{\mathrm{d}(1/\kappa)}{\mathrm{d}\ln R^+} = -\frac{\mathrm{d}(B_i - B_o)}{\mathrm{d}\ln R^+}. \tag{4.22}$$

This is exactly the criterion for the neglected terms in equation (4.10) to vanish identically (i.e. $S_i f_i - S_o f_o \equiv 0$). Therefore the solution represented by equations (4.18) to (4.22) is, indeed, the first-order solution for the velocity profile in the overlap layer at finite, but large, Reynolds number. Clearly when y^+ is too big or $\overline{y}$ is too small for a given value of R^+, the inequalities of equations (4.12) and (4.13) cannot be satisfied. Since all the derivatives with respect to R^+ must vanish as $R^+ \to \infty$ (AIP), the outer range of the inner overlap solution is unbounded in the limit, while the inner range of the outer one is bounded only by $\overline{y} = -\overline{a}$.

Equation (4.22) is invariant to transformations of the form $R^+ \to D_s R^+$ where D_s is a scale factor which ensures that the functional dependence is independent of the particular choice of the outer length scale (e.g. diameter versus radius). Thus the velocity profile in the overlap layer is logarithmic, but with parameters which depend on the Reynolds number, $D_s R^+$. The functions $\kappa(D_s R^+)$, $B_i(D_s R^+)$ and $B_o(D_s R^+)$ must be determined either empirically or from a closure model for the turbulence. Regardless of how they are determined, the results must be consistent with equation (4.22).

5. A solution for the Reynolds number dependence

From equation (4.22) it is clear that if either $B_i - B_o$ or $1/\kappa$ are given, then the other is determined (to within an additive constant). Since there is only one unknown function, it is convenient to transform equation (4.22) using the function

$$H(D_s R^+) \equiv \left(\frac{1}{\kappa} - \frac{1}{\kappa_\infty}\right) \ln D_s R^+ + (B_i - B_o), \tag{5.1}$$

where $H = H(D_s R^+)$ remains to be determined. If $H(D_s R^+)$ satisfies

$$\frac{1}{\kappa} - \frac{1}{\kappa_\infty} = \frac{\mathrm{d}H}{\mathrm{d}\ln D_s R^+} \tag{5.2}$$

then equation (4.22) is satisfied. It follows immediately that

$$\frac{1}{g} = \frac{U_c}{u_*} = \frac{1}{\kappa_\infty} \ln D_s R^+ + H(D_s R^+). \tag{5.3}$$

Thus the Reynolds number dependence of the single function $H(D_s R^+)$ determines that of κ, $B_i - B_o$ and g.

The conditions that both $B_{i\infty}$ and $B_{o\infty}$ be finite and non-zero require that:
either

B_i, B_o and κ remain constant always;

or

(i) $1/\kappa \to 1/\kappa_\infty$ faster than $1/\ln D_s R^+ \to 0$, and
(ii) $H(D_s R^+) \to H_\infty =$ constant.

Obviously from equation (5.1),

$$H_\infty = B_{i\infty} - B_{o\infty}. \tag{5.4}$$

It is also clear from the constraint equation that the natural variable is $\ln D_s R^+$. Since this blows up in the limit as $R^+ \to \infty$, H can at most depend on inverse powers

of $\ln D_s R^+$. Thus the expansion of H for large values of $\ln D_s R^+$ must be of the form

$$H(D_s R^+) - H_\infty = \frac{A}{[\ln D_s R^+]^\alpha}\left[1 + \frac{A_1}{\ln D_s R^+} + \frac{A_2}{(\ln D_s R^+)^2} + \cdots\right]. \tag{5.5}$$

Note that conditions (i) and (ii) above imply that $\alpha > 0$. Although only the leading term will be found to be necessary to describe the data, the rest will be carried in developing the theoretical relations below.

Substituting equation (5.5) in equation (5.3) yields

$$\frac{U_c}{u_*} = \frac{1}{\kappa_\infty}\ln D_s R^+ + [B_{i\infty} - B_{o\infty}] + \frac{A}{[\ln D_s R^+]^\alpha}\left[1 + \frac{A_1}{\ln D_s R^+} + \frac{A_2}{(\ln D_s R^+)^2} + \cdots\right]. \tag{5.6}$$

As $R^+ \to \infty$ this reduces to the classical solution of Millikan (1938). This is reassuring since Millikan's analysis is an infinite Reynolds number analysis of inner and outer profiles scaled in the same way. (Note that this was not true for the boundary layer: the Clauser/Millikan analysis assumed the same scaling laws applied as for the channel/pipe. George & Castillo argued from the Reynolds-averaged equations that they had to be different, hence the different conclusions.)

The Reynolds number variation of $1/\kappa$ and $B_i - B_o$ can be obtained immediately from equations (5.1), (5.2) and (5.5) as

$$\frac{1}{\kappa} - \frac{1}{\kappa_\infty} = -\frac{\alpha A}{(\ln D_s R^+)^{1+\alpha}}\left[1 + \left(\frac{1+\alpha}{\alpha}\right)\frac{A_1}{\ln D_s R^+} + \left(\frac{2+\alpha}{\alpha}\right)\frac{A_2}{(\ln D_s R^+)^2} + \cdots\right] \tag{5.7}$$

and

$$(B_i - B_o) - (B_{i\infty} - B_{o\infty}) = \frac{(1+\alpha)A}{(\ln D_s R^+)^\alpha}\left[1 + \left(\frac{2+\alpha}{1+\alpha}\right)\frac{A_1}{\ln D_s R^+} + \left(\frac{3+\alpha}{1+\alpha}\right)\frac{A_2}{(\ln D_s R^+)^2} + \cdots\right]. \tag{5.8}$$

Figure 3 shows the friction data of the superpipe experiment of Zagarola & Smits (1998*a*). As the investigators themselves have pointed out, careful scrutiny reveals that the data do not fall on a straight line on a semi-log plot, so a simple logarithmic friction law with constant coefficients does not describe all the data to within the accuracy of the data itself. In particular, a log which attempts to fit all of the data dips away from it in the middle range. On the other hand, a log law which fits the high Reynolds number range does not fit the low, or vice versa. Figure 3 shows two curves: the first represents a regression fit of equation (5.6) with only the leading term (i.e. $A_1 = A_2 = 0$), while the second shows only the asymptotic log form of equation (5.6). The former provides an excellent fit to the data for all Reynolds numbers and asymptotes exactly to the latter, but only at much higher Reynolds numbers. The differences, although slight, are very important since they entirely determine (or reflect) the Reynolds number dependence of the parameters $1/\kappa$, B_i and B_o. The last of these will be seen later to be especially sensitive to this dependence. Clearly the simplest of the proposed forms of H captures the residual Reynolds number dependence, while simply using constant coefficients does not.

The values obtained for the asymptotic friction law parameters using optimization techniques are $\kappa_\infty = 0.447$, $B_{i\infty} - B_{o\infty} = 8.45$, while those describing the Reynolds number dependence are $A = -0.668$ and $\alpha = 0.441$. The higher-order terms in equation (5.5) were ignored, and will be throughout the remainder of this paper. The same optimization techniques showed no advantage in using values of the parameter D_s different from unity, hence $D_s = 1$ to within experimental error. Note that the

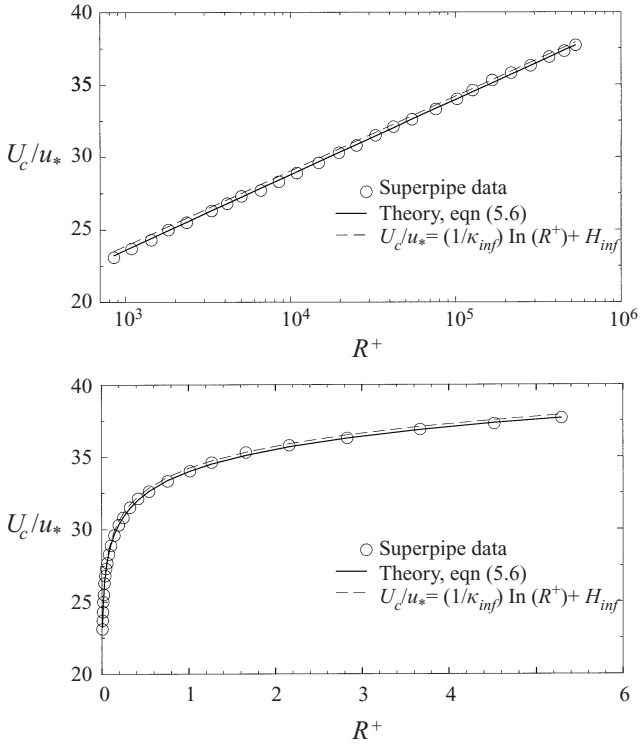

FIGURE 3. Variation of U_c/u_* with $R^+ = Ru_*/\nu$.

values of $B_{i\infty}$ and $B_{o\infty}$ cannot be determined individually from the friction data, only their difference. Nominal values for κ and $B_i - B_o$ are approximately 0.445 and 8.20 respectively, the former varying by less than 0.5% and the latter by only 1% over the entire range of the data. These values differ only slightly from the values determined by Zagarola (1996) (0.44 and 7.8, respectively) and Zagarola & Smits (1998*a*) (0.436 and 7.66, respectively) using the velocity profiles alone and assuming that the asymptotic state had been reached. In fact it will be shown later from the velocity profiles that B_i is independent of Reynolds number and approximately equal to 6.5. Thus only B_o significantly changes with Reynolds number and then only by about 5% over the range of the data, but even this variation will be seen to be quite important for the outer profile. Note that the friction law is independent of the parameter a.

All the parameters are remarkably independent of the particular range of data utilized. For example, after optimizing the parameters in equation (5.6) for the friction data of all 26 different Reynolds numbers available, the highest 15 Reynolds numbers could be dropped before a new optimization would even change the second digit of the values of the parameters cited above. This suggests strongly, contrary to the suggestion of Barenblatt *et al.* (1997) (see also Barenblatt & Chorin 1998; Smits & Zagarola 1998, for response), that the superpipe data are in fact a smooth curve, uncontaminated by roughness. If the analysis developed herein is correct, then the reason these authors had a problem with the superpipe data is obvious: the data vary logarithmically as derived here, and not according to their conjectured power law.

For the boundary layer the friction data are not as reliable as those reported here,

so the functional form of $h(\delta^+)$ had to be inferred by GC after a variety of attempts to describe the variation of the exponent in a power law description of the velocity profile in the overlap region. Interestingly, the value for α obtained here is almost exactly the value obtained for the boundary layer data (0.46 versus 0.44). Even more intriguing is that both of these are nearly equal to the values found for κ_∞ and $1/(\gamma_\infty C_{i\infty})$. It is not yet clear whether this is of physical significance, or whether it is just coincidence.

6. Single-point second-order turbulence quantities

Unlike the boundary layer, where the continued downstream evolution imposes certain similarity constraints, for pipe and channel flows there is only a single velocity scale so all quantities must scale with it. An immediate consequence of this is that all quantities scaling with the velocity only will have logarithmic profiles in the overlap region. (It is straightforward to show this by the same procedures applied above to the mean velocity.)

For example, in inner variables, the Reynolds stress profiles are given by

$$\langle -u_m u_n \rangle^+ = \frac{\langle -u_m u_n \rangle}{u_*^2} = A_{imn}(R^+) \ln (y^+ + a^+) + B_{imn}(R^+). \tag{6.1}$$

As for the velocity, the parameters A_{imn} and B_{imn} are functions of the Reynolds number and asymptotically constant. Note that the offset a^+ has been assumed to be the same as for the velocity, although this needs to be subjected to experimental verification.

The Reynolds shear stress is particularly interesting since for it more information can be obtained from the mean momentum equation. In the overlap region in the limit as $R^+ \to \infty$, both equations (2.2) and (2.3) reduce to

$$0 = \frac{\partial \langle -uv \rangle}{\partial y} \tag{6.2}$$

or in inner variables,

$$0 = \frac{\partial \langle -uv \rangle^+}{\partial y^+}. \tag{6.3}$$

It follows from substituting the 1, 2-component of equation (6.1) that

$$0 = \frac{A_{i12}}{y^+ + a^+}. \tag{6.4}$$

It is immediately clear that equation (6.3) can be satisfied only if $A_{i12} \to 0$ as $R^+ \to \infty$. A similar argument for the outer profile implies $A_{o12} \to 0$. Thus to leading order, the Reynolds shear stress profile in the overlap region is independent of y; however, the remaining parameters B_{i12} and B_{o12} are only asymptotically constant. From equation (2.4) it is clear that $B_{i12} \to 1$, but only in the limit. Since $\langle -uv \rangle \to u_*^2$ is also the inner boundary condition on equation (2.2), $B_{o12} \to 1$ in the limit also.

Another quantity of particular interest is the rate of dissipation of turbulence energy per unit mass, ϵ. For the inner part of the flow, the appropriate dissipation scale must be u_*^4/ν on dimensional grounds, since there are no other possibilities. In the outer layer in the limit of infinite Reynolds number, the dissipation is effectively inviscid (as discussed in § 7 below), so it must scale as u_*^3/R. (Note that this only means that profiles scaled as $\epsilon\nu/u_*^4$ vs. y^+ and $\epsilon R/u_*^3$ vs. $\overline{y}$ will collapse in the limit

of infinite Reynolds number in the inner and outer regions, respectively.) It is easy to show by the methodology applied to mean velocity and Reynolds stresses above that the dissipation profile in the overlap region is given by a *power law* with an exponent of -1. Thus

$$\epsilon^+ = \frac{\epsilon v}{u_*^4} = \frac{E_i(R^+)}{y^+ + a^+} \tag{6.5}$$

and

$$\overline{\epsilon} = \frac{\epsilon R}{u_*^3} = \frac{E_o(R^+)}{\overline{y} + \overline{a}}, \tag{6.6}$$

where both E_o and E_i are asymptotically constant. It has again been assumed that the origin shift a is the same as for the mean velocity. For the dissipation, this can be justified using the production equals dissipation limit as shown in the § 8.

7. The effect of Reynolds number on the overlap region

The asymptotic values of the parameters established for the friction law will be used below to calculate the values of κ, B_i and B_o for each Reynolds number of the superpipe data. Only either of the B one need be established from the experiments since their difference is known from equation (5.1). Before carrying out a detailed comparison with the velocity data, however, it is useful to first consider exactly which region of the flow is being described by the overlap profiles. Also of interest is the question of how large the Reynolds number must be before the flow begins to show characteristics of the asymptotic state.

The overlap layer identified in the preceding sections can be related directly to the averaged equations for the mean flow and the Reynolds stresses. From about $y^+ > 30$ out to about the centre of the flow, the averaged momentum equation is given approximately by

$$0 = -\frac{1}{\rho}\frac{\mathrm{d}P}{\mathrm{d}x} + \frac{\partial\langle -uv\rangle}{\partial y}. \tag{7.1}$$

It has no explicit Reynolds number dependence; and the Reynolds shear stress drops linearly all the way to the centre of the flow (see Perry & Abell 1975). Inside about $\overline{y} = 0.1$ and outside of $y^+ = 30$, however, the Reynolds shear stress is very nearly constant. In fact, at infinite Reynolds number the pressure gradient term vanishes identically in the constant Reynolds shear stress region and the mean momentum equation reduces to

$$0 = \frac{\partial\langle -uv\rangle}{\partial y}. \tag{7.2}$$

At finite (but large) Reynolds numbers this region is similar to the developing boundary layer where the Reynolds stress is effectively constant. Obviously *the overlap region corresponds to this constant Reynolds shear stress layer* since the Reynolds shear stress gradient is the common term to both inner and outer momentum equations. Note that many low Reynolds number experiments do not have a region where the Reynolds stress is even approximately constant because the pressure gradient term is not truly negligible. Hence it is unreasonable to expect such experimental profiles to display any of the characteristics of the overlap described above, except possibly in combination with the characteristics of the other regions (e.g. through a composite solution).

Even when there is a region of reasonably constant Reynolds stress, however, there remains the Reynolds number dependence of $\langle -uv \rangle$ itself. And it is this weak Reynolds number dependence which is the reason that κ, B_i, and B_o are only asymptotically constant. The origin of this weak Reynolds number dependence (which is well-known to turbulence modellers) can be seen by considering the Reynolds transport equations. For the same region, $y^+ > 30$, the viscous diffusion terms are negligible (as in the mean momentum equation), so the Reynolds shear stress equations reduce approximately to (Tennekes & Lumley 1972)

$$0 = -\left(\left\langle p\frac{\partial u_i}{\partial x_k}\right\rangle + \left\langle p\frac{\partial u_k}{\partial x_i}\right\rangle\right) - \left[\langle u_i u_2\rangle\frac{\partial U_k}{\partial x_2} + \langle u_k u_2\rangle\frac{\partial U_i}{\partial x_2}\right] - \frac{\partial\langle u_i u_k u_2\rangle}{\partial x_2} - \epsilon_{ik}, \quad (7.3)$$

where $U_i = U\delta_{i1}$. Thus viscosity does not appear directly in any of the single-point equations governing the overlap region, nor in those governing the outer layer.

Viscosity, however, can be shown to play a crucial role in at least a portion of the constant stress layer, even at infinite Reynolds number. The reason is that the length scales at which the dissipation, ϵ_{ik}, actually takes place depend on the local turbulence Reynolds number, $R_t = q^4/\nu\epsilon$. For $R_t > 5000$ approximately, the energy dissipation is mostly determined by the large energetic scales of motion. These scales are effectively inviscid, but control the energy transfer through nonlinear interactions (the energy cascade) to much smaller viscous scales where the actual dissipation occurs (Tennekes & Lumley 1972). When this is the case, the dissipation is nearly isotropic so $\epsilon_{ik} \approx 2\epsilon\delta_{ik}$. Moreover, ϵ can be approximated by the infinite Reynolds number relation: $\epsilon \sim q^3/L$, where L is a scale characteristic of the energy-containing eddies. The coefficient has a weak Reynolds number dependence, but is asymptotically constant. Thus, the Reynolds stress equations themselves are effectively inviscid, but only exactly so in the limit. Note that in this limit the Reynolds shear stress has no dissipation at all, i.e. $\epsilon_{12} = 0$.

At very low turbulence Reynolds number, however, the dissipative and energy-containing ranges nearly overlap, and so the latter (which also produce the Reynolds shear stress) feel directly the influence of viscosity. In this limit, the energy and dissipative scales are about the same, so the dissipation is more reasonably estimated by $\epsilon \sim \nu q^2/L^2$, where the constant of proportionality is of order 10. The dissipation tensor, ϵ_{ik} is anisotropic and ϵ_{12}, in particular, is non-zero. (Hanjalic & Launder 1974, for example, take $\epsilon_{12} = (-\langle u_1 u_2\rangle\epsilon/q^2)$.)

For turbulence Reynolds numbers between these two limits, the dissipation will show characteristics of both limits, gradually making a transition from $\epsilon \sim \nu q^2/L^2$ to $\epsilon \sim q^3/L$ as R_t increases. This is felt by the Reynolds stresses themselves, which will show a strong Reynolds number dependence. Obviously, in order to establish when (if at all) parts of the flow become Reynolds number independent, it is necessary to determine how the local turbulence Reynolds number varies across the flow.

Over the outer part of the pipe (which is most of it), $L \approx R/2$ and $q \approx 3u_*$. So when $R^+ > 3000$, the dissipation in the outer flow is effectively inviscid. Above this value the mean and turbulence quantities in the core region of the flow should show little Reynolds number dependence. This is indeed the case as illustrated by figure 2. The outer region cannot, of course, be entirely Reynolds number independent, except in the limit, and this residual dependence manifests itself in the overlap layer in the slow variations of κ and B_o, for example.

The near-wall region is considerably more interesting since in it the scales governing the energy-containing eddies are constrained by the proximity of the wall. Hence, the turbulence Reynolds number, R_t, depends on the distance from the wall, y. In fact,

$R_t \sim y^+$ with a coefficient of about 18 (Gibson 1997); so, in effect, y^+ is the turbulence Reynolds number. Two things are then immediately obvious:

First, as the Reynolds number increases more of the pipe (in outer variables) will become effectively inviscid and will be governed by the inviscid dissipation relation. Correspondingly, the properly scaled mean and turbulence quantities in at least the outer part of the overlap layer (say, an *inertial sublayer*) will become Reynolds number independent, albeit very slowly. This cannot be reached until the layer is governed by the infinite Reynolds number dissipation relation and its coefficient has reached the limiting value. Obviously this can happen only when there is a substantial inertial sublayer satisfying $y^+ > 300$ (approximately) and for which the mean pressure-gradient term is negligible, typically $\overline{y} < 0.1$. Thus the asymptotic limits are realized only when $300\nu/u_* \ll 0.1R$ or $R^+ \gg 3000$. Therefore below $R^+ = 30\,000$ approximately, even this inertial sublayer should display a Reynolds number dependence, not only in κ, B_o, and B_i, but correspondingly in the behaviour of $\langle u^2 \rangle$, $\langle uv \rangle$, etc. The lower limit of this inertial sublayer also corresponds (for the same reasons) to the place where a $k^{-5/3}$-region should begin to be observed in the energy spectra.

Second, at the bottom of the overlap region (or the constant Reynolds shear stress layer) there will always be a *mesolayer*† below about $y^+ \approx 300$ in which the dissipation can never assume the character of a high Reynolds number flow, no matter how high the Reynolds number becomes. This is because the dissipation (and Reynolds stress as well) can never become independent of viscosity in this region. Even though the single-point Reynolds-averaged equations are inviscid above $y^+ \approx 30$, the multi-point equations are not! This fact is well-known to turbulence modellers (see Hanjalic & Launder 1974), but the consequences for similarity theory and asymptotic analyses do not seem to have been noticed previously. It is particularly important for experimentalists who have routinely tried to apply asymptotic formulae to data in this region, wrongly believing the mesolayer to be the inertial sublayer.

Thus, as illustrated in figure 4, the constant stress layer has two separate regions, each having their own unique character: the *constant Reynolds shear stress* (*or overlap*) *region* and *the viscous sublayer* where the viscous stress is also important. Each of these has two subregions. The overlap region consists of an *inertial sublayer* ($y^+ > 300$, $\overline{y} < 0.1$) which is nearly inviscid, and a *mesolayer* ($30 < y^+ < 300$) in which the viscous stresses are negligible, but in which viscosity acts directly on the turbulence scales producing the Reynolds stresses. The viscous sublayer is composed of a buffer layer ($3 < y^+ < 30$) where the Reynolds stress and viscous stress both act directly on the mean flow, and the linear sublayer near the wall ($y^+ < 3$) where the viscous stresses dominate. Of these four regions, the inertial sublayer will be the last to appear as the Reynolds number is increased. Thus, the overlap layer itself will be most difficult to identify at the modest Reynolds numbers of most laboratory experiments, unless the properties of the mesolayer are known. In the next section it will be argued that, in fact, it is the offset parameter a^+ which accounts for it. Thus the inertial sublayer can readily be identified as the region for which $y^+ \gg |a^+|$ and the velocity profile in it is primarily a log profile in y alone, the contribution of the offset being negligible, i.e. $\ln(y + a) \approx \ln y$. Attempts to identify logarithmic behaviour inside $y^+ = 300$ from

† This appropriates a term from R. R. Long in a presentation at a Naval Hydrodynamics meeting at Washington, DC, in 1976 (see also Long & Chen 1981) who argued strongly for its existence, but from entirely different physical and scaling arguments which we find untenable. Despite the skepticism which greeted his ideas, Long's instincts were correct.

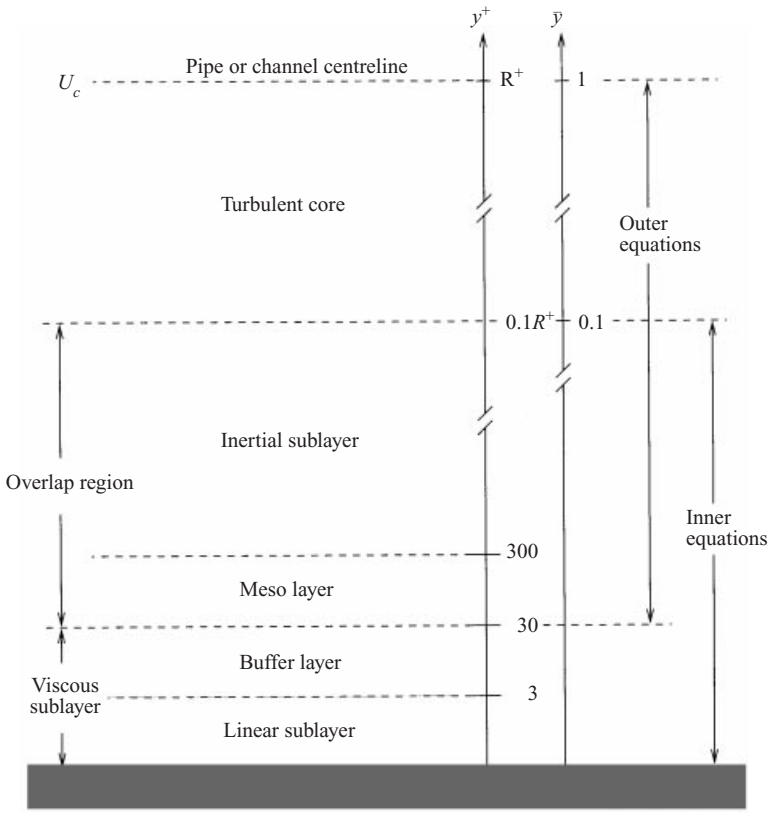

FIGURE 4. Schematic showing various regions and layers of pipe and channel flows.

straight lines on semi-log plots of u^+ versus y^+ are of little use if the theory presented herein is correct because of the presence of a. They will, of course, always succeed as a local approximation, but coefficients so determined will be incapable of extension to higher values of y^+ as the Reynolds number is increased. And this is indeed the history of attempts to identify the log layer and its parameters from such data.

8. A mesolayer interpretation of a^+

As noted in § 4 above, Squire (1948) was apparently the first to notice the need for the offset coordinate $y^+ + a^+$. The basis of his argument was that the mixing length could not be taken as proportional to y alone, since the physics incorporated in it could not account for the thickness of the viscous sublayer. Although the overlap analysis presented here depends on different closure assumptions, the argument concerning invariance to coordinate origin presented earlier is not much different, in principle at least. The preceding section argues for the existence of a mesolayer below the usual inertial layer in which the well-known scale separation of the energy and dissipative eddies cannot exist. The purpose of this section is to show how these last two ideas are related.

The overlap solution of equation (4.19) can be expanded for values of $y^+ \gg |a^+|$:

$$\frac{U}{u_*} = f_i(y^+, R^+) = \frac{1}{\kappa}\left\{[\ln y^+ + \kappa B_i] + \frac{a^+}{y^+} - \frac{1}{2}\frac{a^{+2}}{y^{+2}} + \frac{1}{3}\frac{a^{+3}}{y^{+3}} + \cdots\right\}. \qquad (8.1)$$

For $y^+ \gg 2|a^+|$, this can be approximated by the first three terms as

$$\frac{U}{u_*} \approx \frac{1}{\kappa} \ln y^+ + B_i + \frac{a^+}{\kappa y^+}. \tag{8.2}$$

An equivalent expansion in outer variables is given by

$$\frac{U - U_c}{u_*} \approx \frac{1}{\kappa} \ln \overline{y} + B_o + \frac{\overline{a}}{\kappa \overline{y}}. \tag{8.3}$$

Equations (8.2) and (8.3) are useful for three reasons: First, they are an excellent approximation to the overlap solutions for values of $y^+ > 2|a^+|$ (or $\overline{y} > 2|\overline{a}|$). Second, they are easier to incorporate into a composite solution which includes the viscous sublayer than is the overlap solution itself since they do not have the singularity at $y^+ = -a^+$ (cf. GC). Third, the inner variable version can be shown to offer useful insight into the role of the parameter a^+ as accounting for the mesolayer.

In the overlap region the turbulence energy balance reduces to production equals dissipation, i.e. in inner variables, $P^+ \approx \epsilon^+$. This is exactly true in the limit of infinite Reynolds number, and approximately true at finite Reynolds numbers for $30 < y^+ < 0.1R^+$. It follows immediately by substitution of the overlap solutions for velocity, Reynolds stress and dissipation for P^+ and ϵ^+ that

$$P^+ = \frac{B_{i12}}{\kappa(y^+ + a^+)} = \epsilon^+ = \frac{E_i}{(y^+ + a^+)}. \tag{8.4}$$

It is clear that the offset a^+ must be the same for both velocity and dissipation, as assumed earlier. Hence $E_i = B_{i12}/\kappa \to 1/\kappa$, at least in the limit as $R^+ \to \infty$ since $B_{i12} \to 1$.

Therefore, in this limit the dissipation and velocity derivative profiles are identical (as noted earlier) and equal to the derivative of equation (4.19) with respect to y^+, i.e.

$$\epsilon^+ = \frac{1}{\kappa(y^+ + a^+)} = \epsilon_o^+ f_T(y^+), \tag{8.5}$$

where

$$\epsilon_o^+ \equiv \frac{1}{\kappa y^+} \tag{8.6}$$

and

$$f_T \equiv \left[1 + \frac{a^+}{y^+}\right]^{-1} \approx 1 - \frac{a^+}{y^+}, \tag{8.7}$$

where the higher terms in the expansion in a^+ have been neglected. This is identical to the form used by many turbulence modellers for wall-bounded flows (cf. Reynolds 1976; Hanjalic & Launder 1974) to account empirically for the change in the character of the dissipation near the wall since $R_t \approx 18y^+$ as noted earlier. Thus the interpretation of a^+ as a mesolayer parameter is obvious since it, in effect, modifies the dissipation (and hence the velocity profile) near the wall. The suggested value of $a^+ = -8$ accomplishes this.

A similar form of f_T is obtained if the power law profile of GC for the boundary layer is expanded, even though the form of ϵ_o is different. Interestingly, if the order of argument is reversed and any of the simple dissipation models (e.g. Reynolds 1976) are used to deduce the mesolayer contribution to the velocity profile for the boundary layer, they produce a y^{+-1} additive instead of the $y^{+\gamma-1}$ required. Obviously these

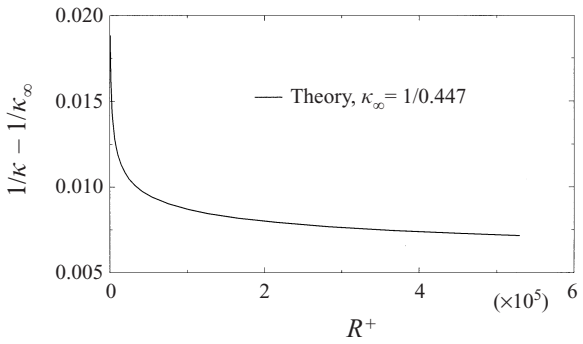

FIGURE 5. Variation of $1/\kappa - 1/\kappa_\infty$ with R^+, $\kappa_\infty = 0.447$.

simple turbulence models, as currently posed, are consistent with the theory developed herein only for homogeneous flows, although the difference is slight.

Note that the common practice of choosing the model constants in equation (8.7) to produce a log profile at $y^+ \approx 30$ is clearly wrong if the proposed theory is correct, since this is the location where the mesolayer only begins. As noted in § 7, the mesolayer ends at $y^+ \approx 300$, and the inertial sublayer begins. It follows that a^+ should be chosen to 'turn off' the low Reynolds number contribution at about this point (for increasing y^+) and 'turn on' the $\ln y$ solution.

9. The superpipe velocity data

Now that the approximate region of validity of the overlap solution has been established as $30 < y^+ < 0.1R^+$ it is possible to test the theoretical profiles and the proposed layer model for the Reynolds number dependence. If they are correct, only an independent determination of either B_i or B_o is necessary to completely specify the profile, the rest of the parameters having been determined from the friction data. Since the superpipe experiments have a substantial range satisfying the conditions for the existence of the inertial sublayer ($300 < y^+ < 0.1R^+$), it should be possible to establish the value of B_i (or B_o) independent from the mesolayer. Also it should be possible to determine whether the parameter a^+ accounts for the mesolayer behaviour, at least for those data sets where data are available below $y^+ = 300$.

For all of the data sets it appears that $B_i = 6.5$ is nearly optimal (at least for values of $R^+ > 850$, the lowest available in this experiment), so that for the remainder of this paper it will be assumed that $B_i = B_{i\infty}$. This value is close to the value of 6.15 determined by Zagarola & Smits (1998*a*), who assumed κ fixed at 0.436. Since the difference, $B_{i\infty} - B_{o\infty} = 8.45$, was established from the friction data, it follows that $B_{o\infty} = -1.95$. (Note, however, that the DNS channel data below suggest that $B_{o\infty} = -2.1$ and $B_{i\infty} = 6.35$ might be more appropriate, but the evidence is not conclusive yet.)

The constancy of B_i implies that it is B_o which shows all the Reynolds number dependence of the difference given by equation (5.8). Figures 5 and 6 show the theoretical variation of $1/\kappa$ and B_o with Reynolds number (equations (5.1) and (5.2)). Clearly both converge very slowly to their asymptotic values. This has far more relative effect on B_o than it does on $1/\kappa$, however, since B_o has achieved only 85% of its asymptotic value at $R^+ = 10^5$. The observed variation of $1/\kappa$ and B_o and the constancy of B_i can be contrasted with the boundary layer results of George *et al.*

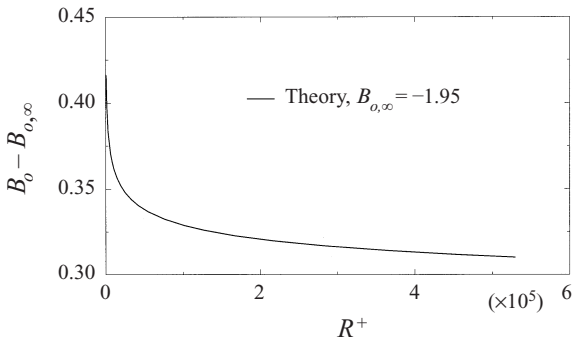

FIGURE 6. Variation of $B_o - B_{o,\infty}$ with R^+, $B_{o\infty} = -1.95$.

(1996) and GC in which C_o, the outer coefficient, was nearly constant while the power exponent γ and the inner coefficient C_i varied over the entire range of Reynolds numbers available.

Therefore the outer profile scaling will show more variation with Reynolds number in the overlap region than the inner where only κ varies. This explains a great deal of the problems historically in establishing what $B_{o\infty}$ is and in determining whether the outer scaling is correct. And it might also explain the conclusion of Zagarola & Smits (1998*a*) that a different scale for the outer flow is required, especially if attention is focused on the overlap region instead of the core region of the flow.

Figures 7 and 8 show representative velocity profiles of the superpipe data at high and low Reynolds numbers, respectively. The profiles scaled in inner variables are shown in the upper plots, and the same data scaled in outer variables are shown in the lower plots. Also shown for each profile are the overlap solutions of equations (4.18) and (4.19) together with equations (5.7) and (5.8). The vertical lines on each profile show the suggested bounds for the two sublayers of the overlap region; in particular, the mesolayer ($30 < y^+ < 300$ or $30/R^+ < \overline{y} < 300/R^+$) and the inertial sublayer ($300 < y^+ < 0.1R^+$ or $300/R^+ < \overline{y} < 0.1$). The limits vary with R^+ for each profile. Note that for the highest Reynolds number plots the data were not measured close enough to the wall to see any of the mesolayer; however, they do show clearly the inertial sublayer. For the lowest Reynolds numbers, enough of the near-wall region was resolved to clearly see the mesolayer, but the extent of the inertial sublayer was limited or non-existent. The theoretical profiles were computed using the measured value of R^+ and assuming $a^+ = 0$, -8, and -16 (or $\overline{a} = 0$, $-8/R^+$, and $-16/R^+$). (As noted above, the value of $B_{o\infty} = -1.95$ is determined since $B_{i\infty}$ has been chosen as 6.5 and $B_{i\infty} - B_{o\infty} = 8.45$ from the friction data.) Therefore there are no adjustable parameters in the outer-scaled plot if a^+ is determined from the inner. Thus these outer profiles provide a completely independent test of the theory (and the data as well).

The value of $a^+ = 0$ corresponds to the inertial sublayer solution only, and as expected describes the data well only in the range of $300 < y^+ < 0.1R^+$. The boundary layer value of $a^+ = -16$ (from the power law) is clearly too large, but then there is no reason to expect it to be the same since the homogeneous pipe and inhomogeneous boundary layer flows are fundamentally different, at least in the outer and overlap regions. The best fit to the DNS channel flow data (see below) above $y^+ \approx 30$ is also $a^+ = -8$. It is possible to fit the data to substantially lower values of y^+ by using different values of a^+, but there appears to be no theoretical justification

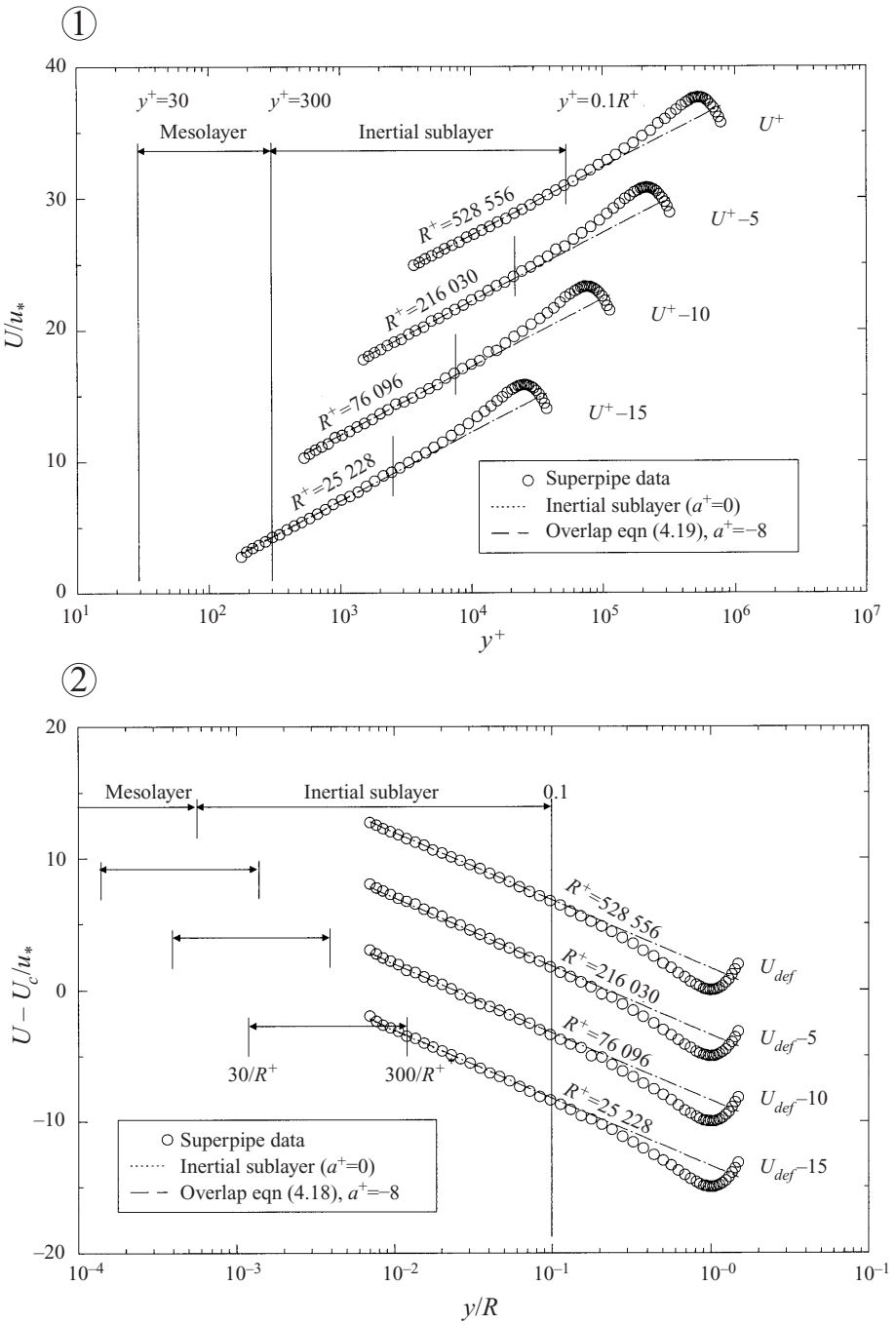

FIGURE 7. Inner and outer profiles at relatively high Reynolds number.

for doing so. Note that the Pitot tube used to make the pipe velocity measurements could be as much as 2% percent too high at $y^+ = 30$ because of the local turbulence intensity there (since $U_{meas}/U \approx 1+[\langle u^2\rangle+\langle v^2\rangle+\langle w^2\rangle]/2U^2$). Additional positive errors probably arise when the probes are closest to the wall because of the asymmetry in the

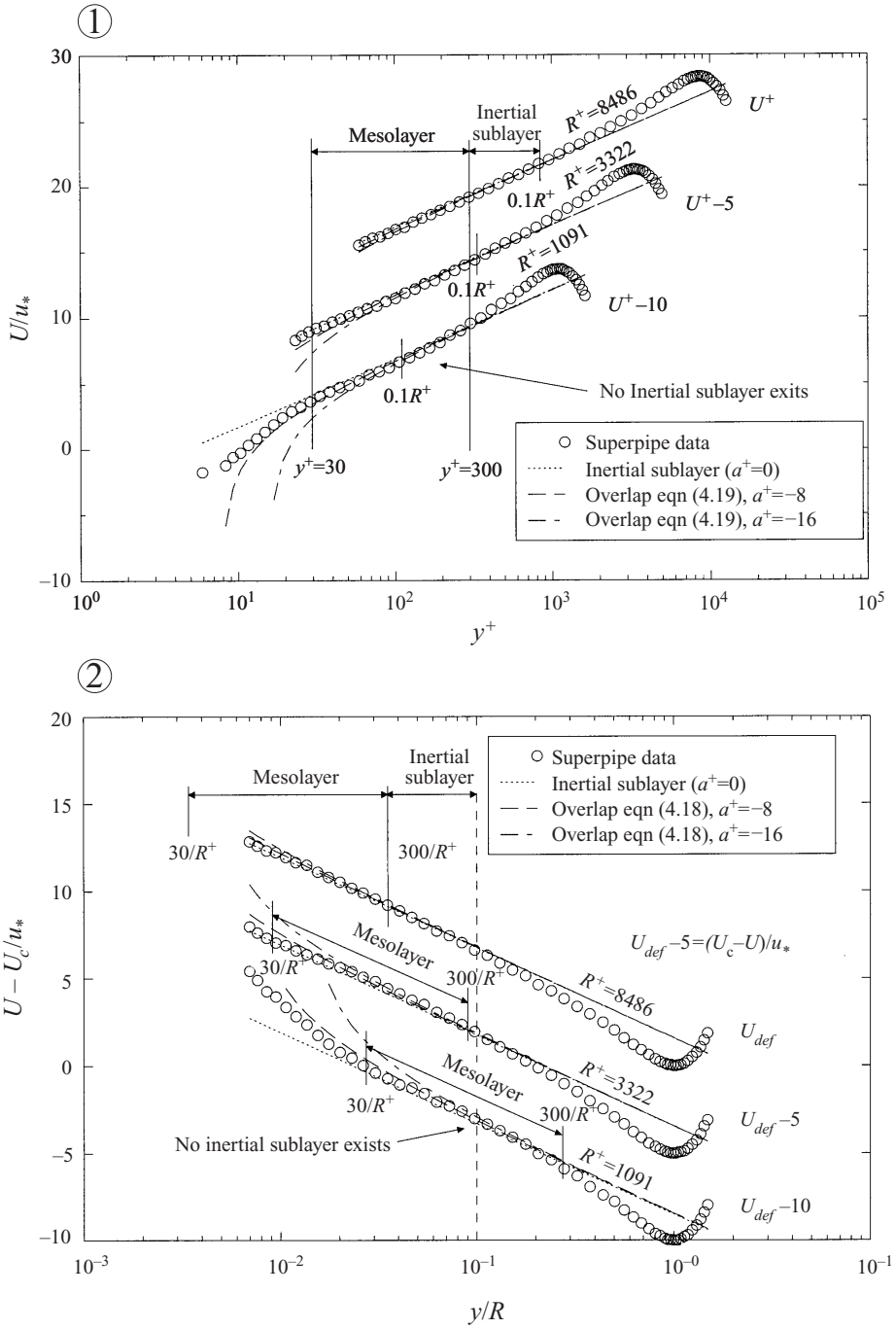

FIGURE 8. Inner and outer profiles at relatively low Reynolds number.

streamline pattern around them. In spite of this, the agreement between experiment and theory over the entire overlap region is particularly gratifying since the velocity data were only used to establish B_i and a^+, the remaining parameters having been entirely determined by the friction data.

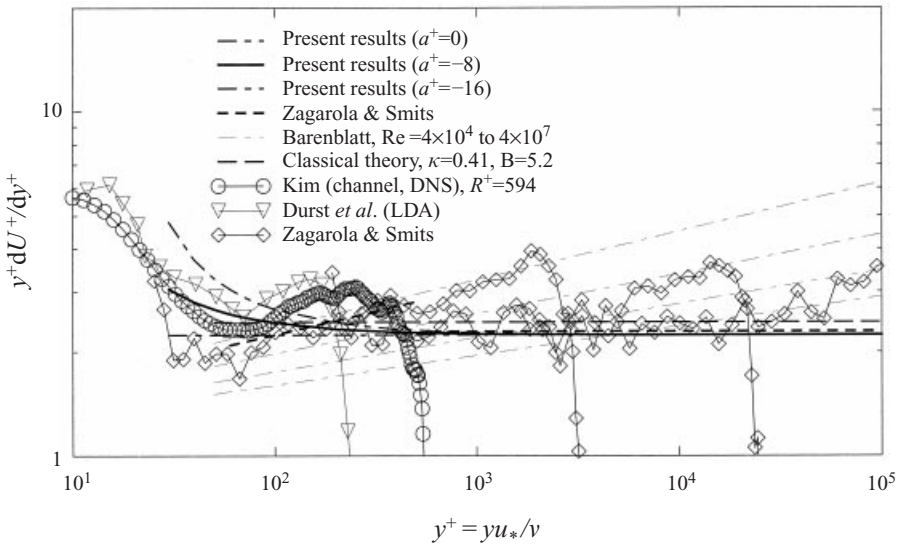

FIGURE 9. Comparison of data and theories for $y^+ du^+/dy^+$ versus y^+.

10. Comparison with other data and theories

Figure 9 shows the profiles of $y^+ dU^+/dy^+$ computed from a number of sources, including the LDA experiment of Durst, Jovanovic & Sender (1995) and the DNS data discussed below. Also shown are a comparison of the present theoretical results with the classical theory and the recent contributions of Zagarola & Smits (1998*a*) and Barenblatt (1993). Only a single $\kappa = 0.447$ is used for the present theory since in inner variables the parameters are nearly constant, but the same three values of a^+ ($-16, -8$, and 0) are shown. The present theory reduces to a constant in these variables only when $a^+ = 0$. On the other hand for large values of y^+, $y^+ dU^+/dy^+ \to 1/\kappa$ for all values of a^+.

The data themselves are not very helpful, especially in the important region from $y^+ = 30$ to 100. The most that can be said from all the data taken together is that the value of a^+ is bounded by these values. A case could be made that -16 is the best choice if the Durst *et al.* data are used. On the other hand, the DNS channel data discussed below would tend to indicate that zero might better.

There are two reasons why the data are problematical. First, the only reliable data in this region are from experiments or simulations in which the Reynolds number is so low that it is impossible to distinguish an overlap region which is reasonably independent of the inner and outer layers. GC dealt with this problem for boundary layers by using semi-empirical inner and outer profiles, then building a composite solution so all the effects could be considered. Obtaining such a composite solution certainly should be a focus of future work. Second, as noted above, this is probably the most difficult region in which to measure accurately. *The errors in measurement with virtually every probe are larger than the differences between the theories which are being compared*, especially for the higher Reynolds numbers. Clearly better experiments and/or simulations at higher Reynolds numbers are necessary.

Figure 10 compares velocity profiles in the overlap region of the present theoretical result with the classical theory and the recent contributions of Zagarola & Smits (1998*a*) and Barenblatt (1993). As noted above there is little difference between the

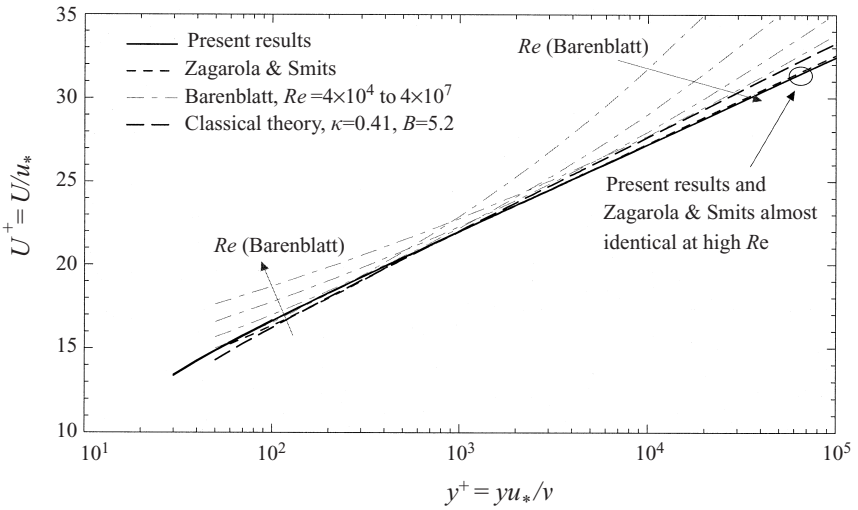

FIGURE 10. Comparison of velocity profiles from various theories.

present results and that of Zagarola & Smits except below $y^+ < 300$–500 for which the latter suggest that a power law region exists. Although it can certainly be argued that a power law fits their low Reynolds number data in this region, there is reason to doubt both the data and the matching procedure used to obtain the power law result. As noted above, measurements with Pitot tubes close to (or even on) the wall might be expected to be in error by the small amounts of interest here. Also, the matching procedure they employ depends on the existence of an outer-scale velocity different from that used to obtain the log region. The outer scale they suggest, $U_c - U_m$, is proportional to u_* in the limit in which the matching is carried out, hence only a log profile can result (cf. Appendix I of GC).

The family of curves due to Barenblatt can at most be argued to fit a region which moves to the right as the Reynolds number is increased. This is exactly what would be expected if the power law form being fitted were not the right choice for an overlap region, a conclusion consistent with the difficulties in this 'theory' in accounting for the superpipe friction data as noted earlier.

11. Channel versus pipe flow

Although both fully developed channel and pipe flows are homogeneous in the stream-wise direction and both scale with u_*, there is no reason, in principle, to expect the outer flow or overlap profiles of channel flow to be the same as for pipe flow. The former is planar and homogeneous in planes parallel to the surface, while the latter is axially symmetric. The geometries are different, but the averaged equations are nearly the same, differing only in the turbulence and viscous transport terms.

The inner regions of both flows have long been known to be quite close (see Monin & Yaglom 1971). In fact, they must be exactly the same in the limit as the ratio of the extent of the viscous sublayer to the pipe radius (or channel half-width) goes to zero. Therefore it is reasonable to hypothesize that the inner regions of both flows be the same. Then the only differences between channel and pipe flows must appear in the outer flow. If this is true, then all of the parameters governing the inner region (including the overlap region in inner variables) must be the same for both

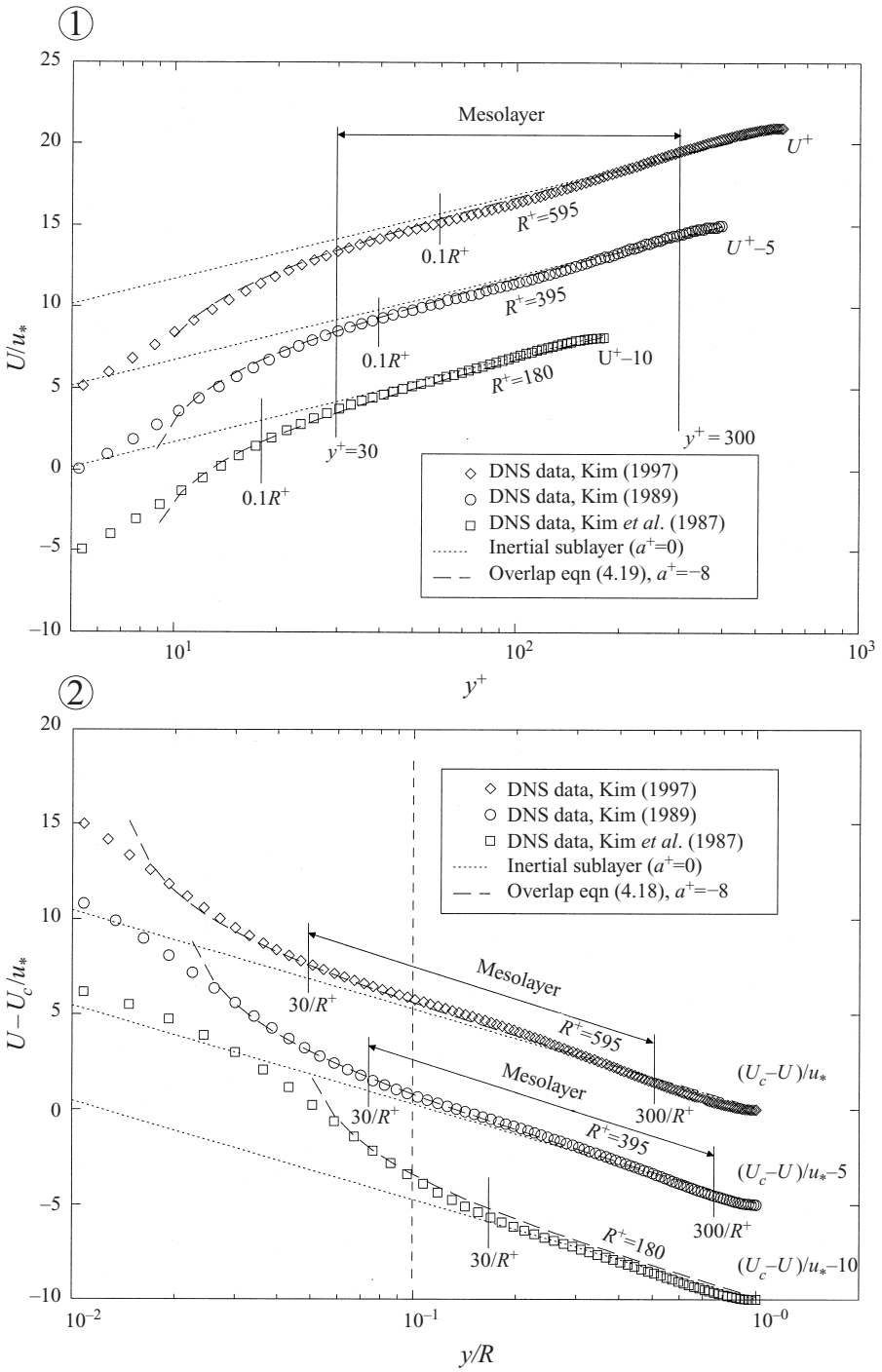

FIGURE 11. Channel flow DNS data of Kim *et al.* (1987), Kim (1989) and Kim (1997).

pipe and channel flows. In particular, the parameters κ and B_i must be the same, as well as their dependence on Reynolds number. Hence even the empirical constants A and α must be identical. Only the parameter B_o and the scale constant D_s can be different. Moreover, since equation (4.22) must be satisfied, the channel flow value

of B_o can at most differ by an additive constant from the pipe flow value, since any other difference would affect the Reynolds-number-dependent relation between κ and $B_i - B_o$.

Figure 11 shows the mean velocity profile data from the channel flow simulations of Kim, Moin & Moser (1987) and Kim (1989) at values of $R^+ = 180$ and 395, where R in this case is taken to mean the channel half-width. Also shown is the profile from data given to us by J. Kim 1997, at $R^+ = 595$.† As before the profiles scaled in inner variables are presented in the upper figure, and the same data in outer variables in the lower. By the criteria established earlier, there should be no region which is described by a simple logarithmic profile alone without the mesolayer contribution, even at the highest Reynolds number. In fact, as is clear from the vertical lines on the plots, there should not even be a mesolayer region in the lowest Reynolds number profile (since $0.1R^+ < 30$).

Nonetheless, the theoretical overlap solution, equation (4.19), with exactly the parameter values used above for the superpipe data, fits all three sets of data in inner variables nicely over the very limited range $30 < y^+ < 0.1R^+$. (In fact, the theoretical curve appears to work well to values of y^+ substantially closer to the wall, even though its use below $y^+ = 30$ cannot be justified theoretically, at least not by the arguments presented earlier.) It is not even necessary to adjust the scale factor D_s which was chosen as unity, just as for the pipe data. This agreement is all the more remarkable because all of the constants have been obtained from the superpipe experiment at much higher Reynolds number.

The theoretical outer velocity profile uses the pipe values for all constants except for $B_{o\infty}$ as noted above. Since $B_{o\infty}$ is quite small for the channel flow, even small uncertainties about its value have a relatively large effect on the outer profile. Therefore the approach taken here has been to first determine $B_{i\infty} - B_{o\infty}$ from the channel friction data, then use the value of $B_{i\infty}$ from the superpipe (since they should be the same as noted above) to determine $B_{o\infty}$ for the channel. Thus the channel flow velocity data scaled in outer variables provide a completely independent test of the theory. Unlike the superpipe data, however, there is much less DNS data available so a sophisticated optimization is not possible. However, there is only a single parameter which needs to be determined. Note that the experimental channel flow data have been avoided entirely because of uncertainties about the shear stress (see Kim *et al.* 1987).

The best overall fit to the friction data, U_c/u_*, is achieved by choosing $B_{i\infty} - B_{o\infty} = 7.0$ with the relative errors being 0.18%, 0.57%, and 1.2% for the Reynolds numbers of 595, 395, and 180 respectively. It follows that $B_{o\infty} = -0.5$.

As shown in the lower plot of figure (11), equation (4.18) provides a reasonable fit to the higher Reynolds number profiles over the same region as for the inner scaling. The fit is especially impressive since there has been no effort to optimize the fit to the velocity profile data. (Recall that all constants but one were determined by the superpipe and the remaining one was chosen from the friction data!) A near perfect fit (not shown) to the two higher Reynolds number profiles can be achieved, however, by using $B_{o\infty} = -0.65$. This will increase the relative error in the friction estimates to 0.089%, 1.3%, and 2.0%, respectively, if B_i is maintained at 6.5. On the other hand, if the value of $B_{i\infty}$ is reduced to 6.35, then both the better friction prediction and the better outer profile fits can be maintained simultaneously (since $B_{i\,\mathrm{inf}} - B_{o\infty} = 7.0$

† The authors are very grateful to Professor Kim for making these data available to us. It has since been published as Moser, Kim & Mansour (1999).

is maintained), but with little relative change to the inner profile. Note that such a value for B_i would be closer to the value of 6.15 suggested by Zagarola & Smits (1998*a*). The authors have resisted the urge to re-analyse the pipe flow data until higher Reynolds number DNS data confirm the need to do so, but it is clear that the only other effect would be to change the pipe flow value of $B_{o\infty}$ from -1.95 to -2.1 which would hardly be noticeable in the plots.

All of the errors between the calculated and DNS values of U_c/u_* are within the uncertainty of the DNS data itself which is estimated at 1–2%. The reason for the larger discrepancy between the lower Reynolds number profiles is probably that the theory is simply being stretched to Reynolds numbers below where it can reasonably be expected to apply. It is clear that the value of $B_{o\infty}$ is substantially lower for the channel than for the pipe, but this was expected since, as noted above, the differences between the two flows should show up only in the outer flow.

The success of the theory developed herein in accounting for the channel flow data using the pipe flow constants should give considerable confidence in the entire theoretical approach. Moreover, it provides an independent confirmation of the values of the constants and the empirical function utilized for the Reynolds number dependence.

12. Summary and conclusions

The asymptotic invariance principle and the deductions from near asymptotics, together with the recognition of the existence of a mesolayer, have provided an excellent description of the mean velocity and skin friction data from fully developed channel and pipe flows over more than three and a half decades in Reynolds number. Specifically the theory describes the velocity profile in the region $30 < y^+ < 0.1R^+$ (or $30/R^+ < \overline{y} < 0.1$) for the superpipe experiment ($850 < R^+ < 530\,000$) and the low Reynolds number DNS data as well ($R^+ = 180$, 395 and 595). Of the five parameters needed to describe the flow, four could be determined only from the friction data alone. Three of these ($\kappa_\infty = 0.447$, $A = -0.67$ and $\alpha = 0.44$) probably apply to any streamwise homogeneous wall-bounded flow. The difference parameter which appears in the friction law, $B_{i\infty} - B_{o\infty}$, is different for pipes and channels (even though $B_{i\infty}$ is the same). From the superpipe experiment, $B_{i\infty} - B_{o\infty} = 8.45$, while from the DNS channel data it was estimated to be 7.0. Both pipe and channel data sets were consistent with constant values of $B_i \approx B_{i\infty} = 6.5$ and $a^+ = -8$. It follows that the outer parameter $B_{o\infty} = -1.95$ for the pipe flow, and -0.5 for the channel flow. A case can also be made that the limiting values of $B_{o\infty}$ should be -2.1 and -0.65 corresponding to $B_{i\infty} = 6.35$, but a final decision can probably not be made until higher Reynolds number DNS data become available.

Unlike the boundary layer, where both Reynolds number effects and the mesolayer were of equal importance in understanding the data, for pipe and channel flows the Reynolds number dependence was found to be slight. In fact, only B_o shows significant variation over the range of the data, and then only about 5%. The variation of the von Kármán parameter, κ, was only about 1%; and both B_i and a^+ were constant to within the accuracy of the data.

On the other hand, the mesolayer concept (and a^+ in particular) proved crucial in understanding where the theory applied and in understanding why previous attempts to verify the log law were less than totally satisfactory. In particular, the overlap mean velocity profile was found to not be a simple logarithm in y, but instead a logarithm in $y + a$. The most important consequence of this is that attempts to establish $\ln y$

behaviour using velocity profile data inside $y^+ = 300$ are doomed to failure and the results misleading unless the mesolayer (and a in particular) are explicitly accounted for. This, of course, explains much of the confusion in the literature about precisely what the log parameters were and where the theory applied – not only was the wrong profile being used, but it was being applied to the wrong region.

It should be noted that for their boundary layer data analysis, George *et al.* (1996) and GC used a procedure which was the reverse of that used here. There a series of careful attempts was first made to obtain directly the variation of the parameters from the velocity profiles, then the friction law was inferred and shown to be in agreement with direct measurements. The fact that the procedure followed here has been equally successful lends credibility to both analyses, especially in view of the importance of the subtle difference between the friction law proposed here and a simple log law with constant coefficients.

There are a number of interesting questions which remain. One of these is whether the mesolayer parameter a^+ is indeed constant, as it appears it might be. This will require accurate measurements of the velocity profile near $y^+ = 30$ at considerably higher Reynolds numbers than has been possible to date. Note that the problem is not with the overall flow Reynolds number (which in the superpipe was certainly adequate), but with the inability to resolve the flow near the wall at the higher Reynolds numbers due to probe size limitations. An obvious solution is a bigger pipe so less absolute resolution is required at a given Reynolds number – a mega-pipe perhaps (or a mighty duct!).

Another question arises from the Reynolds number dependence itself which is nearly negligible for channel and pipe, but crucial for boundary layer flows. Is this a subtle consequence of the homogeneity of the former and inhomogeneity of the latter, or is it simply a reflection of the differing inner and outer velocity scales for the boundary layer with the consequent Reynolds number dependence? Or are these the same thing? Or is the boundary layer's dependence a residual of the dependence on upstream conditions?

Then there is the fact that the parameter, α, which accounts for the Reynolds number dependence is nearly the same as for the boundary layer, and tantalizingly close to κ_∞ and the boundary layer value of $1/(\gamma_\infty C_{o\infty})$. The possible universality of these is particularly interesting, especially given the agreement between theory and experiment for both the homogeneous and inhomogeneous flows. A consequence of this is that the dissipation profiles for the pipe and the infinite Reynolds number boundary layer are nearly identical throughout the overlap region, even though they differ substantially for the finite Reynolds numbers of experiments. And, of course, this raises the question for the functions H (for the pipe and channel) and h (for the boundary layer) which contain the essential Reynolds number dependence of the flow: Can they (or alternatives) be derived directly from the underlying physics of the flow, perhaps through symmetry considerations of the turbulence dissipative scales or from the multi-point equations?

In conclusion, unlike the classical boundary layer theory which was shown by GC to be fundamentally flawed, the same approach has been able to show that the classical theory for pipe and channel flows is really pretty good. The present analysis has, from purely deductive reasoning using the Reynolds-averaged Navier–Stokes equations, been able to identify why the classical results were not totally successful, and was able to account for recent DNS, LDA and superpipe observations. Thus it would seem that the Navier–Stokes equations indeed apply to turbulence, hardly a novel idea to most, but reassuring nonetheless.

The authors are particularly grateful to J. Kim, L. Smits, and M. Zagarola for making their work available to us, and also to M. Oberlack for helping us understand the need for the origin shift in the overlap analysis. The invitation to participate in the *Disquisitiones Mechanicae 1996* at the University of Illinois, Department of Theoretical and Applied Mechanics did much to focus our thinking and move this work forward. The efforts of Professors R. Adrian, S. Balachandar, R. Moser and especially H. Aref to organize and host it are greatly appreciated.

REFERENCES

Barenblatt, G. I. 1993 Scaling laws for fully developed shear flow. Part 1. Basic hypotheses and analysis. *J. Fluid Mech.* **248**, 513–520.

Barenblatt, G. I. 1996 *Scaling, Self-Similarity, and Intermediate Asymptotics*. Cambridge University Press.

Barenblatt, G. I. & Chorin, A. J. 1998 Scaling of the intermediate region in wall-bounded turbulence: The power law. *Phys. Fluids* **10**, 1043–1044.

Barenblatt, G. I., Chorin, A. J. & Prostokishin, V. M. 1997 Scaling laws for fully developed flow in pipes. *Appl. Mech. Rev.* **50**, 413–429.

Barenblatt, G. I. & Prostokishin, V. M. 1993 Scaling laws for fully developed shear flow. Part 2. Processing of experimental data. *J. Fluid Mech.* **248**, 521–529.

Bush, W. B. & Fendell. F. E. 1974 Asymptotic analysis of turbulent boundary layer and channel flow. *J. Fluid Mech.* **56**, 657–681.

Cole, J. D. & Kevorkian, J. 1981 *Perturbation Methods in Applied Mathematis*. Springer.

Duncan, W. J., Thom, A. S. & Young, A. D. 1970 *Mechanics of Fluids*, 2nd edn. Elsevier.

Durst, F., Jovanovic, J. & Sender, J. 1995 LDA measurement in the near-wall region of a turbulent pipe flow. *J. Fluid Mech.* **295**, 305–335.

Frisch, U. 1995 *Turbulence*. Cambridge University Press.

Gad-el-Hak, M. & Bandyopadhyay, P. R. 1994 Reynolds number effects in wall-bounded flows. *Appl. Mech. Rev.* **47**, 307–365.

George, W. K. 1988 Another look at the log (or is it a power law?) velocity profile for a zero-pressure gradient boundary layer. *Bull. Am. Phys. Soc.* **33** no. 10, 2301.

George, W. K. 1990 Another look at the log (or is it a power law?) velocity profile for a zero-pressure gradient boundary layer *3rd Joint ASME/ASCE Mech. Conf. La Jolla, CA, July 9–12.*

George, W. K. 1995 Some new ideas for similarity of turbulent shear flows. In *Proc. ICHMT Symp. on Turbulence, Heat and Mass Transfer, Lisbon, Portugal (1994)* (ed. K. Hanjalic & J. C. F. Pereira). Elsevier.

George, W. K. & Castillo, L. 1993 Boundary layers with pressure gradient: Another look at the equilibrium boundary layer. In *Near Wall Turbulent Flows* (ed. R. M. C. So), pp. 901–910. Elsevier.

George, W. K. & Castillo, L. 1997 Zero-pressure-gradient turbulent boundary layer. *Appl. Mech. Rev.* **50**, 689–729 (referred to herein as GC).

George, W. K., Castillo, L. & Knecht, P. 1996 The zero pressure-gradient turbulent boundary layer. *Tech. Rep.* TRL-153. Turbulence Research Laboratory, University at Buffalo.

George, W. K., Castillo, L. & Wosnik, M. 1997 A theory for turbulent pipe and channel flows. *Tech. Rep.* 872. Theoretical and Applied Mechanics, University of Illinois at Urbana-Champaign.

George, W. K., Knecht, P. & Castillo, L. 1992 The zero pressure-gradient boundary layer revisited. *13th Symposium on Turbulence*, *Rolla, MO*.

Hanjalic, K. & Launder, B. E. 1974 Contribution towards a Reynolds stress closure for low-Reynolds number turbulece. *Rep.* HTS/74/24. Imperial College.

Kim, J. 1989 On the structure of pressure fluctuations in simulated turbulent channel flow. *J. Fluid Mech.* **205**, 421–451.

Kim, J., Moin, P. & Moser, R. T. 1987 Turbulence statistics in fully developed channel flow at low reynolds number. *J. Fluid Mech.* **177**, 133–166.

Long, R. R. & Chen, T.-C. 1981 Experimental evidence for the existence of the 'mesolayer' in turbulent systems. *J. Fluid Mech.* **105**, 19–59.

Millikan, C. M. 1938 A critical discussion of turbulent flows in channels and circular tubes. In *Proc. 5th Intl Congress of Applied Mechanics*, pp. 386–392. John Wiley and Sons.

Monin, A. S. & Yaglom, A. M. 1971 *Statistical Fluid Mechanics*. MIT Press.

Moser, R. T., Kim, J. & Mansour, N. N. 1999 Direct numerical simulation of turbulent channel flow up to $Re_r = 590$. *Phys. Fluids* **11**, 943–945.

Oberlack, M. 1997 Unified theory for symmetries in plane parallel turbulent shear flows. *Manuscript* 163. Center for Turbulence Research, NASA Ames/Stanford University (also submitted to *J. Fluid Mech.*).

Panton, R. 1990 Scaling turbulent wall layers. *Trans. ASME: J. Fluids Engng* **112**, 425–432.

Perry, A. E. & Abell, C. J. 1975 Scaling laws for pipe-flow turbulence *J. Fluid Mech.* **67**, 257.

Prandtl, L. 1932 Zur turbulenten Stroemung in Rohren und laengs Platten. *Ergeb. Aerodyn. Versuch Goettingen* IV. Lieferung, p. 18.

Reynolds, W. C. 1976 Computation of turbulent flows. *Ann. Rev. Fluid Mech.* **8**, 183–208.

Smits, A. J. & Zagarola, M. V. 1998 Response to: Scaling of the intermediate region in wall-bounded turbulence: The power law (Phys. Fluids 10, 1043 (1998)). *Phys. Fluids* **10**, 1045–1046.

Squire, H. B. 1948 Reconsideration of the theory of free turbulence. *Phil. Mag.* **39** (288), 1–20.

Stanton, T. E. & Pannell, J. R. 1914 Similarity of motion in relation to the surface friction of fluids. *Phil. Trans. R. Soc. Lond.* A **214**, 199.

Tennekes, H. 1968 Outline of a second-order theory of turbulent pipe flow. *AIAA J.* **6**, 1735–1740.

Tennekes, H. & Lumley, J. L. 1972 *A first Course in Turbulence*. MIT Press.

Zagarola, M. V. 1996 Mean flow scaling in turbulent pipe flow. PhD thesis, Princeton University.

Zagarola, M. V. & Smits, A. J. 1998*a* Mean-flow scaling of turbulent pipe flow. *J. Fluid Mech.* **373**, 33–79.

Zagarola, M. V. & Smits, A. J. 1998*b* A new mean velocity scaling for turbulent boundary layers. In *Proc. FEDSM'98, Washington DC*. ASME.